Journal of Medical Systems (2020) 44: 32
https://doi.org/10.1007/s10916-019-1483-2

IMAGE & SIGNAL PROCESSING

# Brain Tumor Detection by Using Stacked Autoencoders in Deep Learning

Javaria Amin[1] · Muhammad Sharif[1] · Nadia Gul[2] · Mudassar Raza[1] · Muhammad Almas Anjum[3] · Muhammad Wasif Nisar[1] · Syed Ahmad Chan Bukhari[4]

Received: 19 February 2019 / Accepted: 14 October 2019 / Published online: 17 December 2019


## Abstract

Brain tumor detection depicts a tough job because of its shape, size and appearance variations. In this manuscript, a deep learning model is deployed to predict input slices as a tumor (unhealthy)/non-tumor (healthy). This manuscript employs a high pass filter image to prominent the inhomogeneities field effect of the MR slices and fused with the input slices. Moreover, the median filter is applied to the fused slices. The resultant slices quality is improved with smoothen and highlighted edges of the input slices. After that, based on these slices' intensity, a 4-connected seed growing algorithm is applied, where optimal threshold clusters the similar pixels from the input slices. The segmented slices are then supplied to the fine-tuned two layers proposed stacked sparse autoencoder (SSAE) model. The hyperparameters of the model are selected after extensive experiments. At the first layer, 200 hidden units and at the second layer 400 hidden units are utilized. The testing is performed on the softmax layer for the prediction of the images having tumors and no tumors. The suggested model is trained and checked on BRATS datasets i.e., 2012(challenge and synthetic), 2013, and 2013 Leaderboard, 2014, and 2015 datasets. The presented model is evaluated with a number of performance metrics which demonstrates the improved performance.

**Keywords** Stacked sparse autoencoder · Glioma · Softmax · Hidden size · Magnetic resonance images

**Mathematical abbreviations and notations**

| | |
|---|---|
| LGG | Low-grade glioma |
| HGG | High-grade glioma |
| MRI | Magnetic resonance imaging |
| CT | Computed tomography |
| DT | Decision tree |
| LDA | Linear discriminant analysis |
| PNN | Probabilistic neural network |
| SSAE | Stacked sparse auto encoder |
| NN | Neural networks |

This article is part of the Topical Collection on *Image & Signal Processing*

✉ Muhammad Sharif
muhammadsharifmalik@yahoo.com; sharif@ciitwah.edu.pk

Javaria Amin
javeriacomsat@gmail.com

Nadia Gul
mrsnadiagul@gmail.com

Mudassar Raza
mudassarraza@ciitwah.edu.pk

Muhammad Almas Anjum
almasanjum@yahoo.com

Muhammad Wasif Nisar
wasifnisar@gmail.com

Syed Ahmad Chan Bukhari
bukharis@stjohns.edu

[1] Department of Computer Science, COMSATS University Islamabad, Wah Campus, Islamabad, Pakistan

[2] Department of radiology, Wah Medical College, POF Hospital, Wah Cantt, Rawalpindi, Punjab, Pakistan

[3] College of EME, NUST, Rawalpindi, Punjab, Pakistan

[4] Division of Computer Science, Mathematics and Science, Collins College of Professional Studies, St. John's University, New York, USA

| | |
|---|---|
| MPSO | Modified particle swarm optimization |
| PTPSA | Piece-wise triangular prism surface area |
| FCM | Fuzzy C-means |
| KNN | k-nearest neighbor |
| ABC | Artificial Bee Colony |
| CNN's | Convolutional neural networks |
| X | Input image |
| H | Hidden Layer |
| C | Kernel vector |
| $\hat{\varphi}_c$ | Average activation value |
| B | bias |
| ε | Activation module |
| δ | Mean squared reconstruction error |
| AE | Autoencoder |
| ρ | Weight decay module |
| γ | Sparsity penalty |
| Φ | Sparsity parameter |
| Ω | Controls weight |
| ∅ | Softmax layer |
| ACC | Accuracy |
| SE | Sensitivity |
| SP | Specificity |
| DSC | Dice similarity coefficient |
| JSI | Jaccard similarity index |
| ROC | Receiver operating characteristic curve |
| JSI | Jaccard similarity index |
| FPR | False positive rate |
| FNR | False negative rate |
| HPF | High pass filter |

## Introduction

The human brain consists of the supportive tissues and nerve cells similar to the meninges and glial cells [1]. They control brainstem activities like breathing, movement of the muscles cerebellum (walk), senses, cerebrum (personality), thinking and emotions. Primary tumors can be benign (non-cancerous) and cancerous cells (malignant). The cancerous cell begins anywhere in the body and also rapidly growing in the brain. The main symptoms of brain tumors rely on their location and size. The common indications are headaches, changes in the mood and personality, trouble in speaking, difficulties in walking, vomiting, and high blood pressure [2]. Ophthalmologists classify the tumors into different grades (I-IV). The common of such tumor types in the children are medulloblastoma, Grade I, Grade II (Glioma) ependymoma and glioma brain stem [3]. Gliomas are kinds of brain lesions with greatest prevalence and death rate [4]. These types of tumors are characterized by high-grade glioma (HGG) and low-grade glioma (LGG) [5, 6]. Even under the treatment, the average patient's survival rate is more than 14 months subsequent to the diagnosis [7]. Recent treatments for tumor detection are radiotherapy, surgery, chemotherapy, and a mixture of them [8, 9].

Characterization of the tumor region is more difficult due to spatially heterogeneity of the neoplastic tissues [10, 11]. Currently, brain tumors diagnosis is based on the histopathologic analysis such as resection and surgical biopsy. But it has some limitations such as interpretation variability and sampling error [3, 12–15]. Several studies use MR spectroscopy for the prediction of a brain tumor [16, 17]. The machine learning approaches are utilized for tumor detection, but accurate tumor detection is an intricate task due to variability in tumor location and appearance [18, 19].

### Major Contribution

The major contribution is described as below:

1. In the preprocessing phase, by using traditional enhancement filters, a new fusion-based method is presented to improve the image presentation. In this stage the input image is resized to 512 × 512 × 1,where, 1 shows the single channel. Then, a high-pass filter is selected to improve the edges of the input image. The output and input image are then fused serially. The final fused image is smoothed by employing 3 × 3 median filter that provides the good effect of the segmentation results as compared with the existing approaches.
2. The seed growing algorithm is employed on the basis of optimal threshold that provides good results for brain tumor segmentation.
3. In classification, fine-tuned stacked sparse autoencoder (SSAE) model is presented. In this phase the segmented images are resized with 32 × 32 × 1 dimension for fast processing. In addition, comprehensive experiments are performed for the selection of the hyperparameters to minimize the error rate.

The remaining of the work is presented as follows: The available literature for brain tumor detection is depicted in Section II. Our work prominent phases are highlighted in Section III. The performance validation is written in Section IV. Section V is the conclusion of this work.

## Related Work

Recently, a variety of work is done for brain tumor diagnosis. The generative method is used for lesion segmentation [20–28]. Fluid vector is used for tumor diagnosis by using T1 weighted images [29]. Diffusion coefficient maps are used for the detection of the tumor by using diffusion tensor images [30]. In handcrafted features extraction methods, intensity features [31], GLCM [32], Gray level gradient distribution, run-

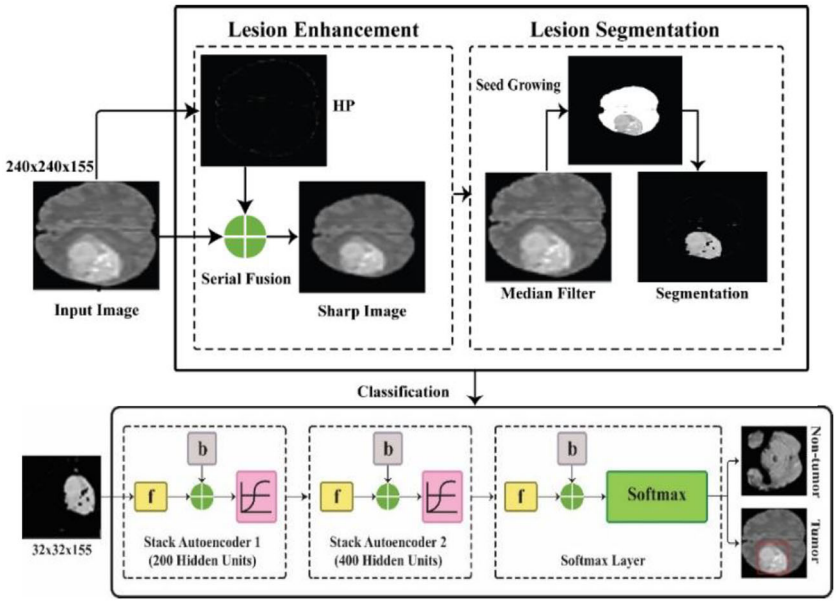


**Fig. 1** Major proposed approach steps

length histogram, gray-Level Co-occurrence matrix, knowledge based (KB), multispectral analysis with k-nearest neighbors (KNN) classifier [33, 34] are utilized for tumor classification. The most used feature extraction methods are GLCM and DWT. The feature reduction methods are also used such as GA and PCA [35]. A lot of work is done for feature extraction/reduction for prediction of the brain tumor, but optimal feature extraction/selection is still a challenging task because number of features increases the correlation. The selection of training/testing samples is also a challenge in achieving good results [36, 37].

Currently, several deep convolutional neural networks (CNN's) [12, 38], DeconvNets (EDD) [39], three-dimensional CNN [13], two pathway cascaded neural network model [40], auto-encoder [41], fully convolutional neural network (FCNN) [15] are used for the analysis of MR images. Two pathway CNN model [12] is employed for the prediction of brain tissues [42]. Binary CNN is utilized for complete tumor region prediction [43]. The patch-based method is utilized for medical image analysis [44]. Deeper CNN model, 3X3 kernel size with few weights are employed for tumor detection [45]. In addition, capsule network is widely utilized [46], where learning is performed through routing agreement process. The capsule network is successful for classification as compared to CNN. The pooling in capsule networks is not performed for down sampling. The fusion of deep learning and handcrafted features can also be utilized for further improvement in tumor classification [47]. To overcome the existing limitations, still there is a need of lightweight methods to diagnose brain tumor more precisely at an early stage and save the radiologist's time as well as increase the patient's survival rate. Therefore, this manuscript presents a lightweight stack sparse auto-encoder (SSAE) method for brain tumor detection in less processing time. Mathematical notations are mentioned in the Table given in appendix at the end of the manuscript.

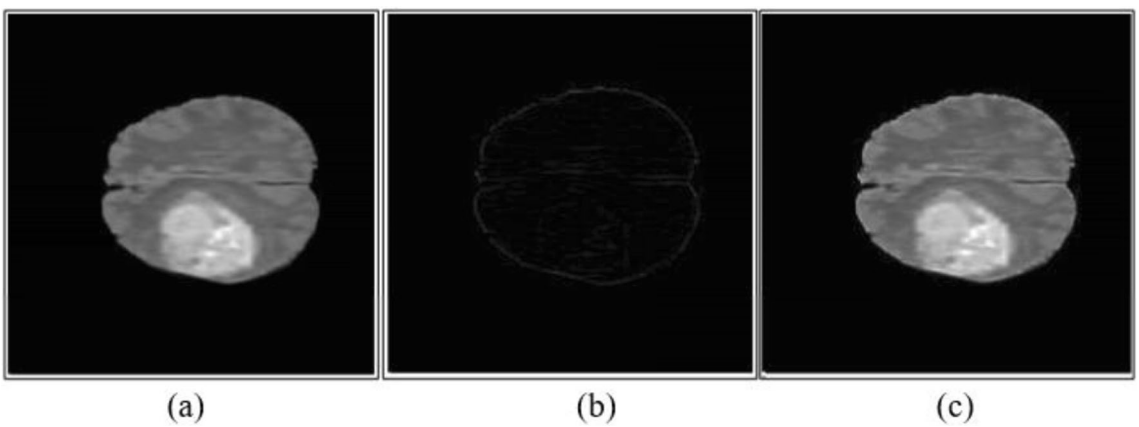


**Fig. 2** Image Sharping (**a**) input (**b**) high pass (**c**) sharper image

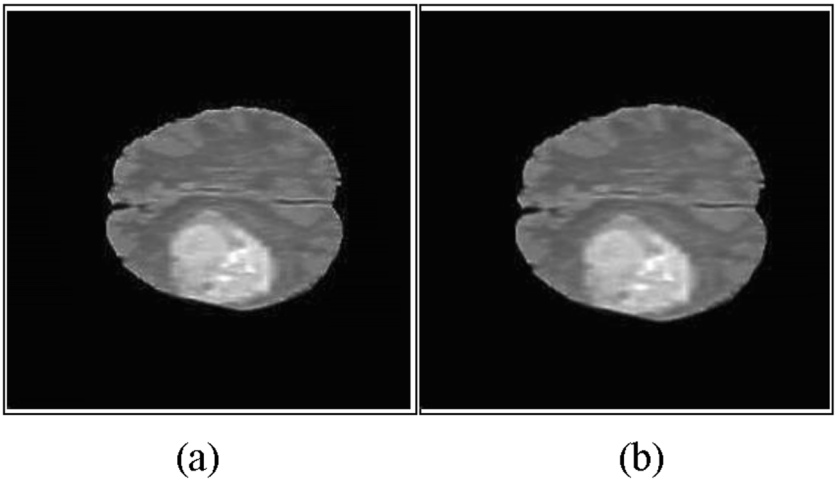


**Fig. 3** Smoothing (**a**) sharper image (**b**) smooth image

## Motivation

This work is motivated by a previous methodology presented in [48]. In that methodology, handcrafted features (geometric) and an SVM classifier are employed for tumor detection. The proposed work of this manuscript utilizes SSAE for acquiring the features and softmax classifier is for tumor prediction.

## Proposed Methodology

The presented approach performs in three different steps. In the first step, high pass [49] and the median filter [50], are chosen to enhance of input images. The seed growing method is used in the second stage to segment the brain tumor. Finally, in the third step, the segmented images are supplied to SSAE [51] model, in which two hidden layers are used that are further concatenated with a softmax layer for classification. Figure 1 shows proposed method steps.

The major contribution is described as below:

- In the initial phase, the high pass filter is employed to improve the edges of the input image. The resultant high-pass filtered outcome is then fused with the input image. The final fused image is smoothed by applying a $3 \times 3$ median filter that provides a good effect on the segmentation results.
- In the classification phase, a deep learning model based on SSAE is fine-tuned by selecting optimized hyperparameters to minimize the error rate.

### Lesion Enhancement Using High Pass Filter

In MR images acquisition process noise appears due to fluctuations of the magnetic field. Therefore, a method is proposed for noise reduction and enhancing the lesion region. In the proposed method, high pass filter (HPF) is selected to highlight the edges in the input I. The sharped image $sh_I$ is

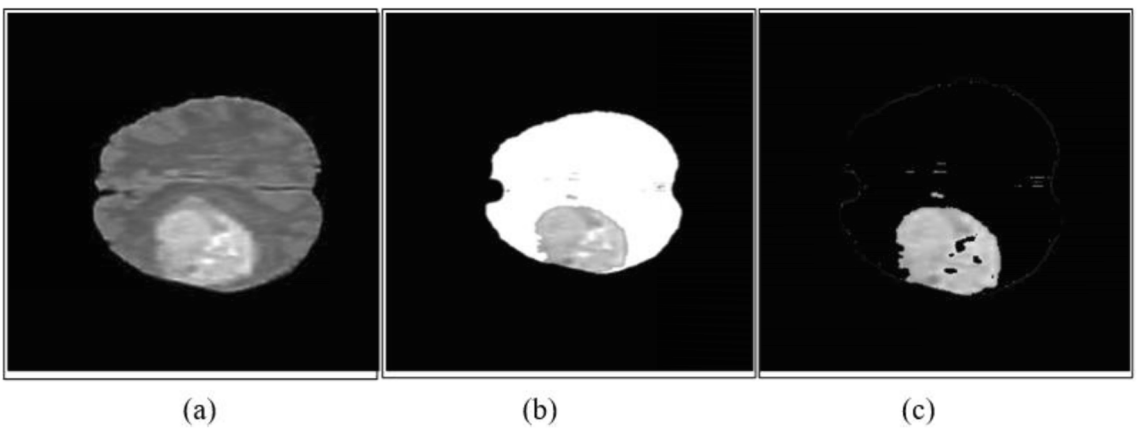


**Fig. 4** Tumor segmentation (**a**) input image (**b**) seed growing (**c**) after applying thresholding

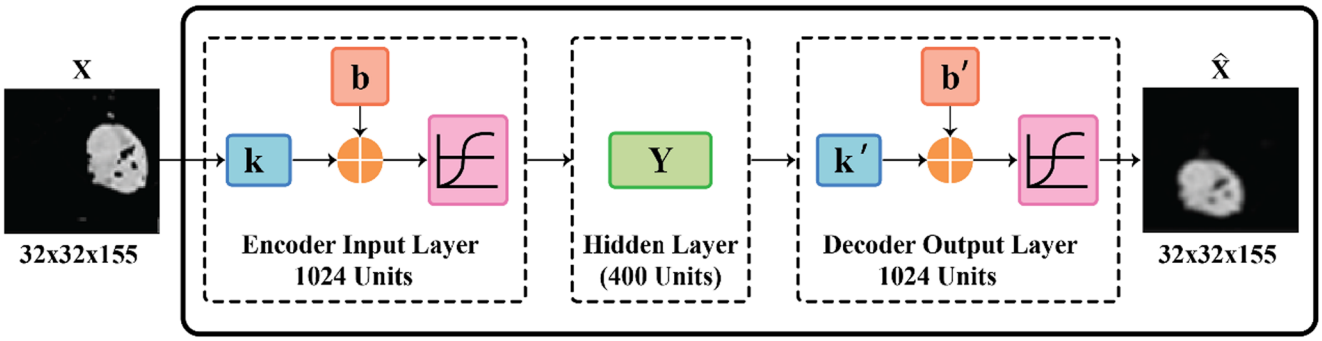


**Fig. 5** A model of an Autoencoder

obtained by combining I with the filtered image $hp_I$ (As Fig. 2 shows).

$$sh_{I(x,y)} = I(x,y) + hp_{I(x,y)} \quad (1)$$

The median filter with 3 × 3 window size is used to smooth the intensities of the sharper image (As Fig. 3 depicts).

## Lesion Segmentation Using Seed Growing Method

Glioma segmentation is performed by using a seed growing approach. When different iterations are completed then the identical pixel values are grouped. This process is repeated until the region stops growing. Eq. (2) mathematically expresses the predicate function $pr_I$ used in seed growing algorithm.

$$pr_{I(x,y)} = \begin{cases} 1 & \text{if the difference between the seed point and current pixels} \le T \\ 0 & \text{otherwise} \end{cases} \quad (2)$$

where T denotes the predefined threshold (As shown in Fig. 4).

## Autoencoders (AE)

The AE neural system works on the basis of unsupervised learning (feed-forward back-propagation). AE performs input images reconstruction and creates the same sized output images. AE process is performed in two stages; such as encoder and decoder stages. Suppose a vector X with the unlabeled sub-inputs denoted as the $I_1, I_2, \ldots, I_p(x_i \in \mathbb{R}^n)$. The Y hidden layers (i.e. $y_1, y_2, \ldots, y_q$ ($y_i \in R^h$,h = total hidden units) that are created through the encoder stage, (As Eq. (3) shows).

$$f(X) = Y = \xi(kX + b) \quad (3)$$

where k and b denote kernel vector and bias respectively. ξ represents the activation module (As define in Eq. 4).

$$\xi(X) = \frac{1}{(1 + e^{-X})} \quad (4)$$

**Table 1** Description of each benchmark datasets (each case has 155 slices)

| BRATS datasets | Cases | |
|---|---|---|
| | LGG | HGG |
| 2012 | 25 | 25 |
| 2012 synthetic | 25 | 25 |
| 2013 | 10 | 20 |
| 2013 Leaderboard | 4 | 21 |
| 2014 | 200 | 200 |
| 2015 | 54 | 220 |

**Table 2** Performance metrics used in this manuscript

| Performance metrics | Equations |
|---|---|
| DCS | $DCS = \frac{2TP}{FP+2TP=+FN}$<br>DCS is used to compute the ratio among the actual tumor and non-tumor pixels that are compared with predicted tumor/non-tumor pixels. |
| SE | $SE = \frac{TP}{TP+FN}$<br>SE is used to calculate the degree of how much method is sensitive to measure the tumor detection rate. |
| SP | $SP = \frac{TN}{TN+FP}$<br>SP is the proportion betweenthe true negative and true positive. |
| ACC | $ACC = \frac{TP+TN}{TP+TN+FP+FN}$<br>ACC is used to compute the degree of correct tumor classification rate. |
| PPV | $PPV = \frac{TP}{TP+FP}$<br>PPV provides a probability to test the positive screening of tumor rate. |
| FPR | FPR = 1-Specificity<br>FPR = is used to compute the ratio of wronglydetected pixels and correctly detected pixels. |
| FNR | FNR = 1-Sensitivity<br>FNR is used to compute the proportion that is positive, but method detects its negative. |
| JSI | $JSI = \frac{TP}{TP+FN+FP}$<br>JSI is used to compute the similarity between the actual tumor pixels and predicted tumor pixels. |

**Table 3** Some hyperparameters combinations during experimentations

| SAE layer 1 | | | | SAE layer 2 | | | | Training error |
|---|---|---|---|---|---|---|---|---|
| HU size | $\mathscr{S}$ | ⊔ | € | HU size | $\mathscr{S}$ | ⊔ | € | |
| **200** | **0.001** | **0.5** | **0.35** | **400** | **0.003** | **4** | **0.25** | **0.0255** |
| 100 | 0.05 | 0.4 | 0.20 | 200 | 0.010 | 3 | 0.3 | 0.0365 |
| 300 | 0.02 | 0.3 | 0.10 | 400 | 0.020 | 4 | 0.4 | 0.0412 |
| 500 | 0.01 | 0.5 | 0.50 | 300 | 0.010 | 4 | 0.4 | 0.0405 |
| 600 | 0.03 | 0.4 | 0.40 | 100 | 0.001 | 5 | 0.5 | 0.0588 |
| 300 | 0.04 | 0.2 | 0.20 | 400 | 0.040 | 2 | 0.2 | 0.0461 |

Figure 5 presents a working of autoencoder. Eq. (5) denotes the reconstructed or decoding phase.

$$\hat{X} = \xi(k'Y + b') \tag{5}$$

Where, $\hat{X}$ denotes the outcome of the reconstructed vector, k illustrates kernel vector, b depicts bias value and ∈ is an error value added during back-propagation.

### Sparse Autoencoder (SAE)

The SAE has sparsity parameters at the concealed layer y. The basic goal of SAE is to measure the optimum kernel values k, k and related bias representation b, b . The optimum values are then acquired through minimizing a cost function (As Eq. (6) shows).

$$SAE = \delta + \Gamma + \omega\zeta \tag{6}$$

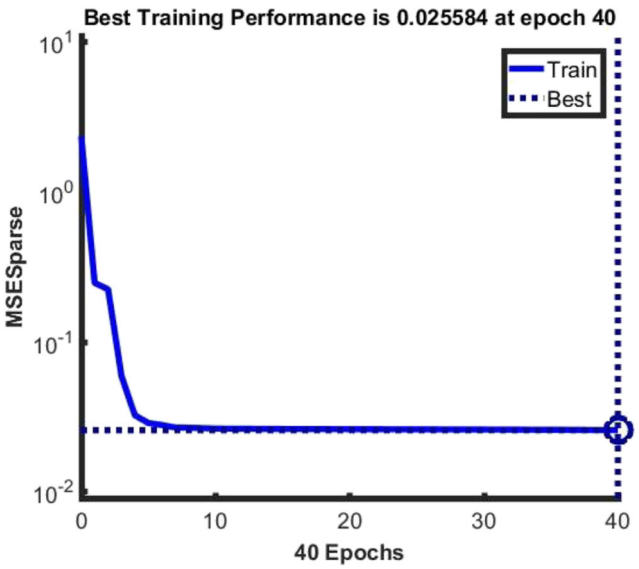


**Fig. 6** Performance of the training data on the basis of MSE and sparsity regulariz

where δ denotes the MSRE (As Eq. (7) depicts).

$$\delta = \frac{1}{s}\sum_{k=1}^{s}\left(\frac{1}{2}\left\|x_k - \hat{x}_k\right\|^2\right) \tag{7}$$

where Γ denotes the weight decay module (also called the L2 regularization weight). This helps to minimize the overfitting (Eq. (8) mentions).

$$\Gamma = \frac{\zeta}{2}\left(\|k\|^2 + \|k'\|^2\right) \tag{8}$$

where ζ shows the sparsity penalty (sparsity regularization) with ω (controls weight), (As Eq. (9) mentions).

$$\zeta = \sum_{k=1}^{r_n} kL\left(\ell \middle\| \hat{\ell}_k\right) \tag{9}$$

where $\ell\rho$ represents sparsity parameter value. The hidden neurons average activation value is denoted as $\hat{\ell}_k$. $r_n$ shows the total neurons of the hidden layer and kL represents the KLKullback-Leibler divergence module.

### Stack Sparse Autoencoder

SSAE [51] stacks SAE1 and SAE2 layers. The first SAE output becomes the input of the next SAE. Instead of using full SAE, shallow SAE is utilized as an inner portion of the stack layer. Shallow SAE indicates the segment of SAE exclusive encoder that is selected for learning and feature acquisition process. Moreover, the features are forwarded to the

**Table 4** Hyper measures for training model

| Layers | Hidden size (units) | Max epochs | L2 weight regularization | Sparsity regularization | Sparsity proportion |
|---|---|---|---|---|---|
| 1 | 200 | 600 | 0.001 | 0.5 | 0.35 |
| 2 | 400 | 600 | 0.003 | 4 | 0.25 |

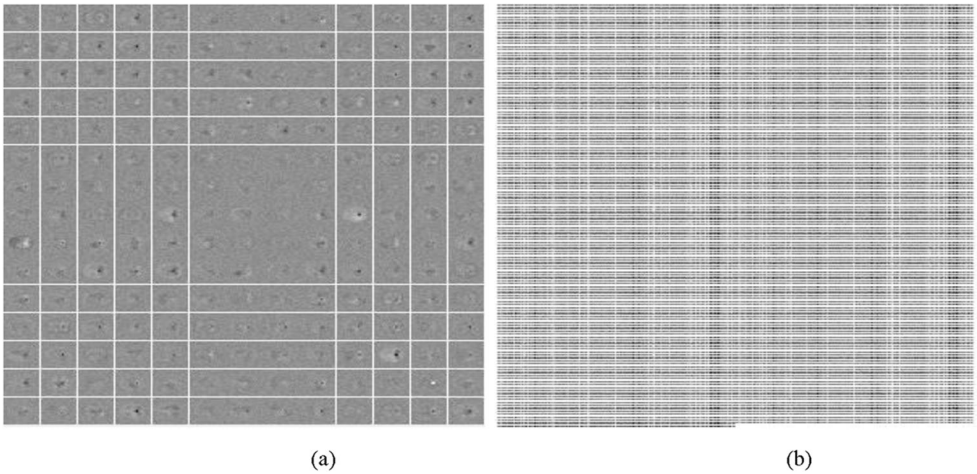


**Fig. 7** Visualization of the first layer on (**a**) 200 hidden units (**b**) 400 hidden units

next layer. The softmax is selected to connect the stacked network. Eq. (10) depicts the stacked network.

$$\mathrm{SSAE} = \psi(k_{SAE2}(k_{SAE1}(X))) \tag{10}$$

$$\psi(Y_i) = \frac{ek_i Y_i}{\sum_{j=1}^{N} ek_j Y_i} \tag{11}$$

where $Y_i$ denotes the output of SSAE.

The softmax classifier $\psi$ is used for classification on the basis of probability. $k_i$ represents $i^{th}$ neuron unit kernel vector and N shows total classes. The output $\psi(Y_i)$ shows the $i^{th}$ class probability.

The segmented images (X) are supplied for training and testing to the SSAE. The input vector size $32 \times 32 \times 155$ is used, where 155 corresponds to a number of slices. The input $32 \times 32$ means that 1024 units are supplied to the SSAE model. This input with 200 hidden units is passed to the SAE1. In SAE1 with bias and weight initial feature vector is created that is passed as an input to the SAE2. In SAE2 400 hidden units are used with bias, weight and different hyperparameters to create a feature vector. The softmax layer is used to perform classification on the basis of feature vector obtained from SAE2.

## Experimental Setup

The autoencoder model is assessed on various BRATS challenge datasets including 2012 (challenge and synthetic), 2013 challenge, 2013 Leaderboard, 2014 challenge, and 2015 challenge. 2012 dataset includes 25 HGG and 25 LGG volumes in training and 25 volumes for the testing phase and each volume is comprises of 155 cuts of the tumor and non-tumor [52]. BRATS 2013 has two subsets including challenge and leaderboard. In 2013 challenge subset 10 LGG, 20HGG cases are used. The leaderboard subset includes 4 LGG and 21 HGG cases [15]. BRATS 2014 includes total 300 cases [53]. BRATS 2015 consists of 384 cases [54]. The explanation across each dataset is illustrated in Table 1. The experiments in this work use MATLAB toolbox 2018 with a Core i7 CPU and 8GB RAM.

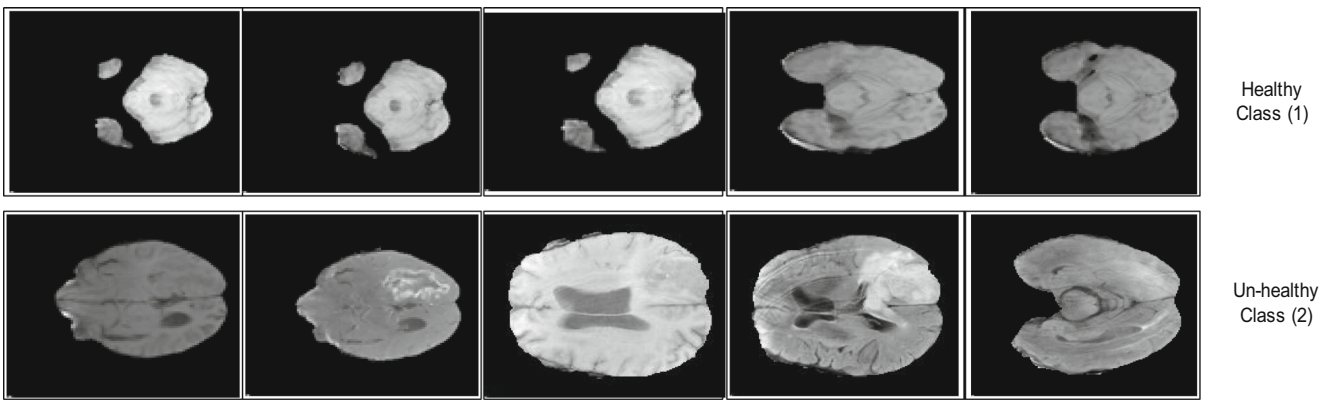


**Fig. 8** Some healthy and unhealthy samples

**Table 5** Results on benchmark datasets

| BRATS datasets | SE | FNR | SP | ACC | AUC | JSI | PPV | FPR | DSC |
|---|---|---|---|---|---|---|---|---|---|
| 2012 | 1.00 | 0.00 | 1.00 | 100% | 1.00 | 1.00 | 1.00 | 0.00 | 1.00 |
| 2012 Synthetic | 0.88 | 0.12 | 1.00 | 90% | 1.00 | 0.89 | 1.00 | 0.00 | 0.94 |
| 2013 | 1.00 | 0.00 | 0.90 | 95% | 0.97 | 0.93 | 0.93 | 0.10 | 0.96 |
| 2013 Leaderboard | 1.00 | 0.00 | 1.00 | 100% | 1.00 | 1.00 | 1.00 | 0.00 | 1.00 |
| 2014 | 0.98 | 0.02 | 0.96 | 97% | 0.99 | 0.97 | 0.98 | 0.04 | 0.98 |
| 2015 | 0.93 | 0.07 | 1.00 | 95% | 0.96 | 0.93 | 1.00 | 0.00 | 0.96 |

## Performance Measures

The brain tumor prediction is evaluated through of confusion matrices (M). M contains total t = 2 classes, where (1) belongs to healthy and (2) belong to unhealthy MR images, that are quantified in terms of overall ACC, SE, SP, DSC, ROC, and JSI. The ROC is provided a ratio among FPR and TPR. These evaluation measures are represented mathematically in Table 2.

The proposed method accurately detect tumor when it achieves the highest quantitative values in term of above-mentioned performance metrics.

## Fine-Tuning of the Proposed Stack Sparse Autoencoder Model

The SSAE model parameters are selected after the experiment and the fine-tuning these parameters are (i) L2 weight regularization ($\mathscr{S}$ ), (ii) sparsity regularization (⊔), (iii) sparsity proportion (€), and (iv) total hidden units (maybe seen Eq. 6–9). The experiment is performed with different combinations of the above-mentioned parameters on SAE 1 &2 layers. The training error vary on these different combination of parameters that is why the combination having minimum training error 0.0255 is selected for further experiments i.e., (200 HU, 0.001 L2 weight regularization, 0.5 sparsity regularization, 0.35 sparsity proportion on SAE layer 1 and 400 HU, 0.03 L2 weight regularization, 4 sparsity regularization, and 0.25 sparsity proportion on SAE layer 2). The detail of the experiments for the selection of optimal hyperparameters with respect to error rate is mentioned in Table 3.

The training performance with selected parameters is shown in Fig. 6 with respect to MSE and sparsity regularization after performing training.

**Table 6** Computational results on BRATS

| BRATS datasets | Time (sec) |
|---|---|
| 2012 Synthetic | 01.725273 |
| 2012 | 01.324803 |
| 2013 | 01.138699 |
| 2013 Leaderboard | 00.800338 |
| 2014 | 26.006808 |
| 2015 | 03.193939 |
| Average time | **04.884200** |

## Experiment #2: Feature-Based Results

The segmented images are passed to SAE layer1 that generated feature vector and passed to SAE layer 2. The SAE layer 2 also generated a feature vector. Then both SAE layer1 and SAE layer 2 features vectors are stacked through softmax classifier for classification. The feature based results are computed with different performance for the classification of tumor/nontumor as mentioned in Table 4. The feature map illustrated in the training process for an input image is depicted in Fig. 7.

Some normal and abnormal samples are illustrated in Fig. 8. The presented procedure outcomes are mentioned in Table 5. Computational time comparison of the presented model between all benchmark datasets is mentioned in Table 6. Evaluation metrics with ROC obtain on benchmark datasets is mention in Fig. 9.

The presented approach comparison in terms of computational time is mentioned in Table 7.

Based on performance evaluation 1.00, 0.94, 0.96, 1.00, 0.98, 0.96 DSCs are obtained on 2012, 2012 Synthetic, 2013, 2013 (Leaderboard), 2014 and 2015 datasets respectively. 2012 and 2013(Leaderboard) perform better as compared to other datasets. Computational time from each benchmark dataset is also measured, where 2013 (Leaderboard) takes 0.800338 s while 2012 Synthetic, 2012, 2013, 2014, and 2015 takes 1.725273 Sec, 1.324803Sec, 1.138699 Sec, 26.006808 Sec and 3.193939 Sec respectively. 2013(Leaderboard) takes less computation time as associated with other benchmark datasets. A comparison of the presented model results with the previous methods is mentioned in Table 8.

The proposed deep learning autoencoder model is compared with eighteen existing methods such as {[12, 14, 64], [13, 15, 40, 52–54, 56–63, 65]}.-Net method achieves 0.86 DSC [64], 3 × 3 Kernel size CNN model obtains 0.78 DSC

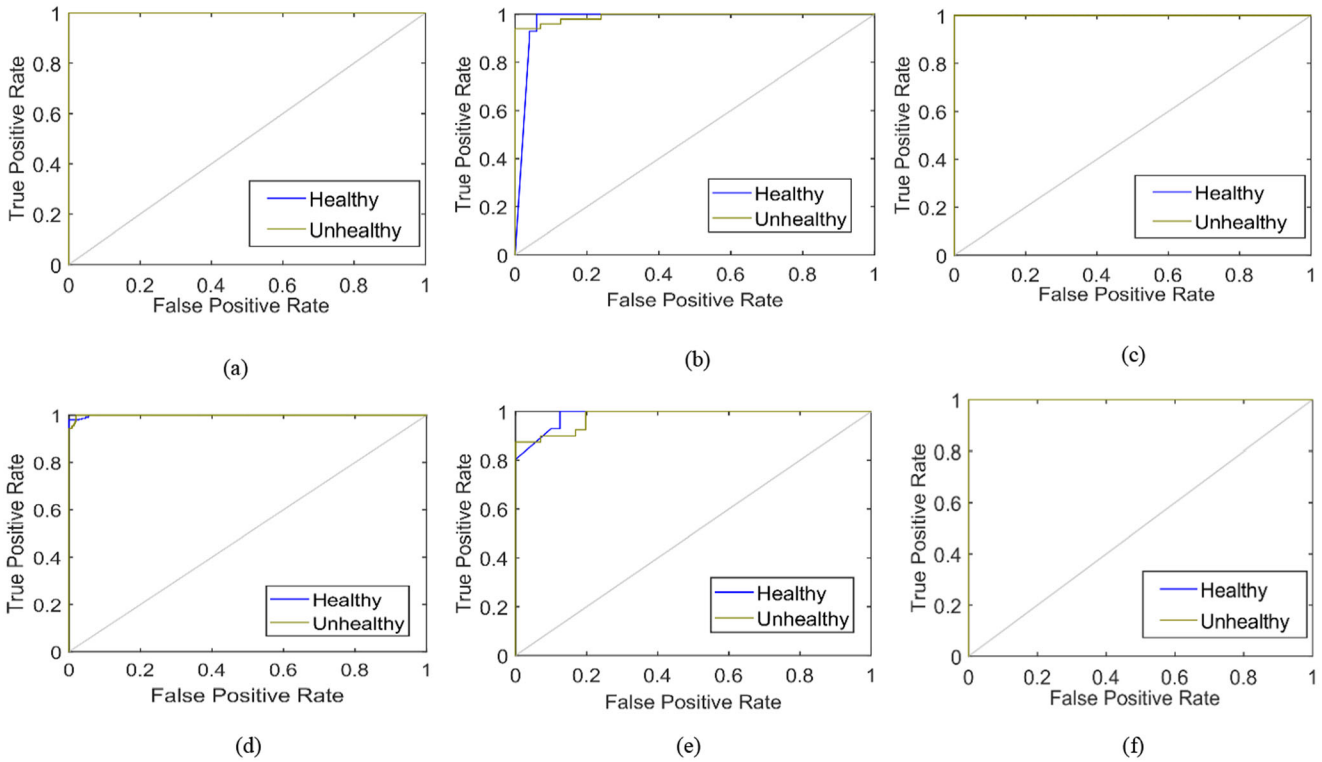


**Fig. 9** ROC results on BRATS datasets (**a**) BRATS 2012 Challenge, (**b**) BRATS 2013 Challenge, (**c**) BRATS 2012 Synthetic, (**d**) BRATS 2014 Challenge, (**e**) BRATS 2015 Challenge, (**f**) BRATS 2013 Leaderboard

[14] and Deep Neural Networks (DNNs) model obtains 0.79 DSC [12]. CNN based approaches are utilized for tumor detection. Our work obtains 0.90 DSC [13]. The MFDFA method is evaluated on the BRATS 2013 challenge. This method achieves 0.90 DSC [53]. Pairwise affinity and superpixel based method achieve a maximum of 0.60 DSC on the BRATS 2012 challenge [56]. Hierarchical classification and regularization based technique obtains a maximum of 0.73 DSC [57]. The classification technique is evaluated on the BRATS 2012 challenge [58]. CNN is employed for tumor detection in BRATS with 0.83 DSC [60]. Extremely randomized trees method obtains 0.83 DSC on 2013 dataset [61]. Generative models are used for brain tumor detection where 0.88 DSC, 0.88 PPV, and 0.89 SE are achieved on the BRATS 2013 challenge [59]. RF method is utilized for tumor detection. This approach obtains 0.87 DSC, 0.85 PPV and 0.89 SE on BRATS 2013 challenge [63].

The above performance evaluations and discussion show that proposed method performed well as compared to existing methodologies.

**Table 7** Time comparison

| Methods | Time |
|---|---|
| [55] | 168.8400 Sec |
| proposed | 004.8842 Sec |

**Table 8** Comparison on various datasets

| BRATS datasets | Methods | DSC | SE |
|---|---|---|---|
| 2012 | [56] | 0.62 | – |
| | [57] | 0.73 | – |
| | [58] | 0.75 | – |
| | **Proposed** | **1.00** | **1.00** |
| 2013 | [14] | 0.88 | 0.89 |
| | [59] | 0.88 | 0.86 |
| | [54] | 0.84 | – |
| | [52] | 0.86 | 0.92 |
| | [12] | 0.88 | 0.87 |
| | [15] | 0.85 | 0.88 |
| | **Proposed** | **1.00** | **1.00** |
| 2013 | [60] | 83.7 ± 9.4 | – |
| | [53] | 0.90 | – |
| | [12] | 0.88 | 0.87 |
| | [14] | 0.88 | – |
| | [61] | 0.83 | – |
| | [58] | 0.88 | – |
| | [59] | 0.88 | 0.89 |
| | [62] | 0.88 | 0.84 |
| | [63] | 0.87 | 0.89 |
| | [52] | 0.86 | 0.92 |
| | **Proposed** | **0.96** | **1.00** |
| 2014 | [53] | 0.89 | 0.84 |
| | **Proposed** | **0.98** | **0.98** |
| 2015 | [64] | 0.86 | – |
| | [14] | 0.78 | – |
| | [12] | 84.7 | 87.6 |
| | [13] | 0.90 | 0.90 |
| | [40] | 0.88 | 0.87 |
| | **Proposed** | **0.96** | **0.93** |

## Conclusion

In this approach, the major steps are performed such as the seed growing method for segmentation and unsupervised SSAE deep learning model for feature extraction. The method is tested on all challenging datasets of BRATS. The average accuracy is 100% on 2012, 90% on 2012 synthetic, 95% on 2013, 100% on Leaderboard 2013, 97% 2014 and 95% 2015 along with AUC 1.00, 1.00, 0.97, 1.00, 0.99 and 0.96 respectively. The overall experimental outcomes conclude that proposed method performs better as compared with the existing approaches.

**Funding** This manuscript receives no funding.

### Compliance with Ethical Standards

**Conflict of Interest** All authors declare that they have no conflict of interest and all contribute equally in this work for results compilation and other technical support.

**Ethical Approval** This work is based on publicly available datasets. This article does not contain any studies with human participants or animals performed by any of the authors.

**Informed Consent** Not Applicable.

## References

1. Anitha, R., and Raja, D. S. S., Development of computer-aided approach for brain tumor detection using random forest classifier. *International Journal of Imaging Systems and Technology* 28:48–53, 2018.
2. Aponte, Raoul J, Patel, Ankur R, Patel, Toral R, "Brain Tumors", Neurocritical Care for the Advanced Practice Clinician:Springer, pp.251–268, 2018, ed.
3. De Wolde, H., Pruim, J., Mastik, M. F., Koudstaal, J., and Molenaar, W. M., Proliferative activity in human brain tumors: Comparison of histopathology and L-(1-11C) tyrosine PET. The Journal of Nuclear Medicine 38:1369, 1997.
4. Bauer, S., Wiest, R., Nolte, L.-P., and Reyes, M., A survey of MRI-based medical image analysis for brain tumor studies. Physics in Medicine & Biology 58:R97, 2013.
5. N. B. Bahadure, A. K. Ray, and H. P. Thethi, "Image analysis for MRI based brain tumor detection and feature extraction using biologically inspired BWT and SVM," *International journal of biomedical imaging,* vol. 2017, 2017.
6. N. Herald Anantha Rufus and D. Selvathi, "Performance analysis of brain tissues and tumor detection and grading system using ANFIS classifier," *International Journal of Imaging Systems and Technology,* vol. 28, pp. 77–85, 2018.
7. Van Meir, E. G., Hadjipanayis, C. G., Norden, A. D., Shu, H. K., Wen, P. Y., and Olson, J. J., Exciting new advances in neuro-oncology: The avenue to a cure for malignant glioma. CA: a cancer journal for clinicians 60(3):166–193, 2010.
8. Tabatabai, G., Stupp, R., Van Den Bent, M. J., Hegi, M. E., Tonn, J. C., Wick, W., and Weller, M., Molecular diagnostics of gliomas: The clinical perspective. Acta neuropathologica 120(5):585–592, 2010.
9. Aronen, H. J., Gazit, I. E., Louis, D. N., Buchbinder, B. R., Pardo, F. S., Weisskoff, R. M., Harsh, G. R., Cosgrove, G., Halpern, E. F., and Hochberg, F. H., Cerebral blood volume maps of gliomas: Comparison with tumor grade and histologic findings. Radiology 191(1):41–51, 1994.
10. Krabbe, K., Gideon, P., Wagn, P., Hansen, U., Thomsen, C., and Madsen, F., MR diffusion imaging of human intracranial tumours. Neuroradiology 39(7):483–489, 1997.
11. Provenzale, J. M., Mukundan, S., and Barboriak, D. P., Diffusion-weighted and perfusion MR imaging for brain tumor characterization and assessment of treatment response. Radiology 239(3):632–649, 2006.
12. Havaei, M., Davy, A., Warde-Farley, D., Biard, A., Courville, A., Bengio, Y., Pal, C., Jodoin, P.-M., and Larochelle, H., Brain tumor segmentation with deep neural networks. Medical image analysis 35:18–31, 2017.
13. Kamnitsas, K., Ledig, C., Newcombe, V. F., Simpson, J. P., Kane, A. D., Menon, D. K., Rueckert, D., and Glocker, B., Efficient multi-scale 3D CNN with fully connected CRF for accurate brain lesion segmentation. Medical image analysis 36:61–78, 2017.
14. Pereira, S., Pinto, A., Alves, V., and Silva, C. A., Brain tumor segmentation using convolutional neural networks in MRI images. IEEE transactions on medical imaging 35(5):1240–1251, 2016.
15. Zhao, X., Wu, Y., Song, G., Li, Z., Zhang, Y., and Fan, Y., A deep learning model integrating FCNNs and CRFs for brain tumor segmentation. Medical image analysis 43:98–111, 2018.
16. Q. Wang, E. K. Liacouras, E. Miranda, U. S. Kanamalla, and V. Megalooikonomou, "Classification of brain tumors using MRI and MRS data," in *Medical Imaging 2007: Computer-Aided Diagnosis*, 2007, p. 65140S.
17. Cho, Y.-D., Choi, G.-H., Lee, S.-P., and Kim, J.-K., 1H-MRS metabolic patterns for distinguishing between meningiomas and other brain tumors. Magnetic resonance imaging 21:663–672, 2003.
18. Li, G.-Z., Yang, J., Ye, C.-Z., and Geng, D.-Y., Degree prediction of malignancy in brain glioma using support vector machines. Computers in Biology and Medicine 36(3):313–325, 2006.
19. Devos, A., Simonetti, A., Van Der Graaf, M., Lukas, L., Suykens, J., Vanhamme, L., Buydens, L., Heerschap, A., and Van Huffel, S., The use of multivariate MR imaging intensities versus metabolic data from MR spectroscopic imaging for brain tumour classification. Journal of Magnetic Resonance 173(2):218–228, 2005.
20. M. Agn, O. Puonti, P. M. af Rosenschöld, I. Law, and K. Van Leemput, "Brain tumor segmentation using a generative model with an RBM prior on tumor shape," in *International Workshop on Brainlesion:* Glioma*,* Multiple Sclerosis*,* Stroke and Traumatic Brain Injuries, 2015, pp. 168–180.
21. Amin, J., Sharif, M., Yasmin, M., and Fernandes, S. L., Big data analysis for brain tumor detection: Deep convolutional neural networks. Future Generation Computer Systems 87:290–297, 2018.
22. Rajinikanth, V., Satapathy, S. C., Fernandes, S. L., and Nachiappan, S., Entropy based segmentation of tumor from brain MR images–a study with teaching learning based optimization. Pattern Recognition Letters 94:87–95, 2017.
23. Fernandes, S. L., Tanik, U. J., Rajinikanth, V., and Karthik, K. A., A reliable framework for accurate brain image examination and treatment planning based on early diagnosis support for clinicians. Neural Computing and Applications:1–12, 2019.
24. V. Rajinikanth, K. P. Thanaraj, S. C. Satapathy, S. L. Fernandes, and N. Dey, "Shannon's Entropy and Watershed Algorithm Based Technique to Inspect Ischemic Stroke Wound," in *Smart Intelligent Computing and Applications*, ed: Springer, 2019, pp. 23–31.
25. Amin, J., Sharif, M., Yasmin, M., Ali, H., and Fernandes, S. L., A method for the detection and classification of diabetic retinopathy using structural predictors of bright lesions. Journal of Computational Science 19:153–164, 2017.

26. Sharif, M., Khan, M. A., Faisal, M., Yasmin, M., and Fernandes, S. L., A framework for offline signature verification system: Best features selection approach. Pattern Recognition Letters, 2018.
27. Naqi, S., Sharif, M., Yasmin, M., and Fernandes, S. L., Lung nodule detection using polygon approximation and hybrid features from CT images. Current Medical Imaging Reviews 14:108–117, 2018.
28. Liaqat, A., Khan, M. A., Shah, J. H., Sharif, M., Yasmin, M., and Fernandes, S. L., Automated ulcer and bleeding classification from WCE images using multiple features fusion and selection. Journal of Mechanics in Medicine and Biology 18:1850038, 2018.
29. Wang, T., Cheng, I., and Basu, A., Fluid vector flow and applications in brain tumor segmentation. IEEE Transactions on Biomedical Engineering 56(3):781–789, 2009.
30. Al-Okaili, R. N., Krejza, J., Woo, J. H., Wolf, R. L., O'Rourke, D. M., Judy, K. D., Poptani, H., and Melhem, E. R., Intraaxial brain masses: MR imaging–based diagnostic strategy—Initial experience. Radiology 243(2):539–550, 2007.
31. Verma, R., Zacharaki, E. I., Ou, Y., Cai, H., Chawla, S., Lee, S.-K., Melhem, E. R., Wolf, R., and Davatzikos, C., Multiparametric tissue characterization of brain neoplasms and their recurrence using pattern classification of MR images. Academic radiology 15(8): 966–977, 2008.
32. Sachdeva, J., Kumar, V., Gupta, I., Khandelwal, N., and Ahuja, C. K., A novel content-based active contour model for brain tumor segmentation. Magnetic resonance imaging 30(5):694–715, 2012.
33. Schad, L. R., Blüml, S., and Zuna, I., IX. MR tissue characterization of intracranial tumors by means of texture analysis. Magnetic resonance imaging 11(6):889–896, 1993.
34. Clark, M. C., Hall, L. O., Goldgof, D. B., Velthuizen, R., Murtagh, F. R., and Silbiger, M. S., Automatic tumor segmentation using knowledge-based techniques. IEEE transactions on medical imaging 17(2):187–201, 1998.
35. Sachdeva, J., Kumar, V., Gupta, I., Khandelwal, N., and Ahuja, C. K., A package-SFERCB-"segmentation, feature extraction, reduction and classification analysis by both SVM and ANN for brain tumors". Applied Soft Computing 47:151–167, 2016.
36. Jiang, J., Wu, Y., Huang, M., Yang, W., Chen, W., and Feng, Q., 3D brain tumor segmentation in multimodal MR images based on learning population-and patient-specific feature sets. Computerized Medical Imaging and Graphics 37:512–521, 2013.
37. A. Ortiz, J. M. Gorriz, J. Ramírez, D. Salas-Gonzalez, and A. s. D. N. I. J. Neurocomputing, "Improving MRI segmentation with probabilistic GHSOM and multiobjective optimization," vol. 114, pp. 118–131, 2013.
38. P. Dvořák and B. Menze, "Local structure prediction with convolutional neural networks for multimodal brain tumor segmentation," in *International MICCAI Workshop on Medical Computer Vision*, 2015, pp. 59–71.
39. Chen, L., Bentley, P., and Rueckert, D., Fully automatic acute ischemic lesion segmentation in DWI using convolutional neural networks. NeuroImage: Clinical, 2017.
40. H. Larochelle and P.-M. Jodoin, "A Convolutional Neural Network Approach to Brain Tumor Segmentation," in *Brainlesion: Glioma, Multiple Sclerosis, Stroke and Traumatic Brain Injuries: First International Workshop, Brainles* 2015*,* Held in conjunction with MICCAI 2015, Munich, Germany, October 5, 2015*,* Revised Selected Papers, 2016, p. 195.
41. X. Chen and E. Konukoglu, "Unsupervised Detection of Lesions in Brain MRI using constrained adversarial auto-encoders," *arXiv preprint arXiv:1806.04972,* 2018.
42. G. B. Huang and V. Jain, "Deep and wide multiscale recursive networks for robust image labeling," *arXiv preprint arXiv: 1310.0354,* 2013.
43. M. Lyksborg, O. Puonti, M. Agn, and R. Larsen, "An ensemble of 2D convolutional neural networks for tumor segmentation," in *Scandinavian Conference on Image* Analysis, 2015, pp. 201–211.
44. V. Rao, M. S. Sarabi, and A. Jaiswal, "Brain tumor segmentation with deep learning," *MICCAI Multimodal Brain Tumor Segmentation Challenge (BraTS),* pp. 56–59, 2015.
45. K. Simonyan and A. Zisserman, "Very deep convolutional networks for large-scale image recognition," *arXiv preprint arXiv: 1409.1556,* 2014.
46. P. Afshar, A. Mohammadi, and K. N. Plataniotis, "Brain tumor type classification via capsule networks," in *2018 25th IEEE International Conference on Image Processing (ICIP)*, 2018, pp. 3129–3133.
47. Akkus, Z., Galimzianova, A., Hoogi, A., Rubin, D. L., and Erickson, B. J., Deep learning for brain MRI segmentation: State of the art and future directions. Journal of digital imaging 30(4): 449–459, 2017.
48. Amin, J., Sharif, M., Yasmin, M., and Fernandes, S. L., A distinctive approach in brain tumor detection and classification using MRI. Pattern Recognition Letters, 2017.
49. D. Matecki, "Ćwiczenie 2: Przetwarzanie i rekonstrukcja sygnałów."
50. J. S. Lim, "Two-dimensional signal and image processing," *Englewood Cliffs, NJ, Prentice Hall,* 1990*, 710 p.,* 1990.
51. Møller, M. F., A scaled conjugate gradient algorithm for fast supervised learning. Neural networks 6:525–533, 1993.
52. G. Urban, M. Bendszus, F. Hamprecht, and J. Kleesiek, "Multimodal brain tumor segmentation using deep convolutional neural networks," *MICCAI BraTS (Brain Tumor Segmentation) Challenge. Proceedings, winning contribution,* pp. 31–35, 2014.
53. S. M. Reza, R. Mays, and K. M. Iftekharuddin, "Multi-fractal detrended texture feature for brain tumor classification," in *Proceedings of SPIE–the International Society for Optical Engineering*, 2015.
54. Menze, B. H., Jakab, A., Bauer, S., Kalpathy-Cramer, J., Farahani, K., Kirby, J., Burren, Y., Porz, N., Slotboom, J., and Wiest, R., The multimodal brain tumor image segmentation benchmark (BRATS). IEEE transactions on medical imaging 34(10):1993–2024, 2015.
55. Chen, S., Ding, C., and Liu, M., Dual-force convolutional neural networks for accurate brain tumor segmentation. Pattern Recognition 88:90–100, 2019.
56. Wu, W., Chen, A. Y., Zhao, L., and Corso, J. J., Brain tumor detection and segmentation in a CRF (conditional random fields) framework with pixel-pairwise affinity and superpixel-level features. International journal of computer assisted radiology and surgery 9(2):241–253, 2014.
57. Bauer, S., Fejes, T., Slotboom, J., Wiest, R., Nolte, L.-P., and Reyes, M., "segmentation of brain tumor images based on integrated hierarchical classification and regularization," in *MICCAI BraTS Workshop*. Nice: Miccai Society, 2012.
58. Huang, M., Yang, W., Wu, Y., Jiang, J., Chen, W., and Feng, Q., Brain tumor segmentation based on local independent projection-based classification. IEEE Transactions on Biomedical Engineering 61(10):2633–2645, 2014.
59. D. Kwon, R. T. Shinohara, H. Akbari, and C. Davatzikos, "Combining generative models for multifocal glioma segmentation and registration," in *International Conference on Medical Image Computing and Computer-Assisted Intervention*, 2014, pp. 763–770.
60. Zikic, D., Ioannou, Y., Brown, M., and Criminisi, A., Segmentation of brain tumor tissues with convolutional neural networks. Proceedings MICCAI-BRATS:36–39, 2014.
61. Goetz, M., Weber, C., Bloecher, J., Stieltjes, B., Meinzer, H.-P., and Maier-Hein, K., Extremely randomized trees based brain tumor segmentation. Proceeding of BRATS challenge-MICCAI:006–011, 2014.
62. D. Kwon, H. Akbari, X. Da, B. Gaonkar, and C. Davatzikos, "Multimodal brain tumor image segmentation using GLISTR,"

*MICCAI Brain Tumor Segmentation (BraTS) Challenge Manuscripts,* pp. 18–19, 2014.

63. Tustison, N. J., Shrinidhi, K., Wintermark, M., Durst, C. R., Kandel, B. M., Gee, J. C., Grossman, M. C., and Avants, B. B., Optimal symmetric multimodal templates and concatenated random forests for supervised brain tumor segmentation (simplified) with ANTsR. Neuroinformatics 13(2):209–225, 2015.
64. H. Dong, G. Yang, F. Liu, Y. Mo, and Y. Guo, "Automatic Brain Tumor Detection and Segmentation Using U-Net Based Fully Convolutional Networks," *arXiv preprint arXiv:1705.03820,* 2017.
65. Haeck, T., Maes, F., and Suetens, P., *"ISLES challenge 2015: Automated model-based segmentation of ischemic stroke in MR images," in International Workshop on Brainlesion: Glioma*. Stroke and Traumatic Brain Injuries: Multiple Sclerosis, 2015, 246–253.